A first-principles study of the influence of helium atoms on the optical response of small silver clusters

M. Pereiro, D. Baldomir, and J. E. Arias

Citation: J. Chem. Phys. **134**, 084307 (2011); doi: 10.1063/1.3556821
View online: https://doi.org/10.1063/1.3556821
View Table of Contents: http://aip.scitation.org/toc/jcp/134/8
Published by the American Institute of Physics

A first-principles study of the influence of helium atoms on the optical response of small silver clusters

M. Pereiro,[1,2,3,a)] D. Baldomir,[1,2] and J. E. Arias[2]
[1]*Departamento de Física Aplicada, Universidade de Santiago de Compostela, Santiago de Compostela E-15782, Spain*
[2]*Instituto de Investigacións Tecnolóxicas, Universidade de Santiago de Compostela, Santiago de Compostela E-15782, Spain*
[3]*Department of Solid State Physics, University of Łódź, ul. Pomorska 149/153, Łódź 90-236, Poland*

(Received 17 September 2010; accepted 31 January 2011; published online 24 February 2011)

Optical excitation spectra of Ag_n and $Ag_n@He_{60}$ ($n = 2, 8$) clusters are investigated in the framework of the time-dependent density functional theory (TDDFT) within the linear response regime. We have performed the *ab initio* calculations for two different exact exchange functionals (GGA-exact and LDA-exact). The computed spectra of $Ag_n@He_{60}$ clusters with the GGA-exact functional accounting for exchange-correlation effects are found to be generally in a relatively good agreement with the experiment. A strategy is proposed to obtain the ground-state structures of the $Ag_n@He_{60}$ clusters and in the initial process of the geometry optimization, the He environment is simulated with buckyballs. A redshift of the silver clusters spectra is observed in the He environment with respect to the ones of bare silver clusters. This observation is discussed and explained in terms of a contraction of the Ag–He bonding length and a consequent confinement of the *s* valence electrons in silver clusters. Likewise, the Mie–Gans predictions combined with our TDDFT calculations also show that the dielectric effect produced by the He matrix is considerably less important in explaining the redshifting observed in the optical spectra of $Ag_n@He_{60}$ clusters. © *2011 American Institute of Physics*. [doi:10.1063/1.3556821]

I. INTRODUCTION

The term cluster is often used to designate a three-dimensional assembly of atoms, and it represents a form of matter with structure and properties lying somewhere between the atoms and the bulk crystals. Specially, the transition-metal (TM) clusters play a dominant role in cluster physics[1] because they exhibit increasingly interesting structural, electronic, catalytic, as well as optical properties.[2,3] Recently, the biomedicine community has recognize their importance for applications such as therapeutical drug delivery, hyperthermic treatment for malignant cells, and magnetic separation of labeled cells among others.[4,5]

Advances in laser and supersonic cluster beam devices over the last years have produced a flood of new and exciting results about the structure and optical properties of TM clusters. Within the subfield devoted to the study of the optical properties of TM clusters, certainly one of the most active and intellectually exciting area is the study of noble metal clusters and more specifically the study of silver clusters. The main reason argued by theoreticians is that the accurate description of ground and excited electronic states of silver clusters is feasible since their electronic structures lie between the alkali metals and the transition metals and consequently some of their physical and chemical properties can be qualitatively understood by their single valence *s* electrons.[6] Thus, it is a good starting point to consider these clusters as the keystone for assessing the validity of new theoretical and experimental methods. Some state-of-the-art techniques that have been successfully employed to calculate the optical spectra of clusters are time-dependent density functional theory (TDDFT),[7] quantum Monte Carlo calculations,[8] configuration interaction based quantum chemistry methods,[9] or a Green's-function-based "quasiparticle" methodology[10] while from the experimental side, the silver clusters have been mainly studied by photodepletion spectroscopy on cluster-rare gas complexes,[11] and in an embedding rare gas matrix.[6] More recently, helium nanodroplet isolation spectroscopy has proven to be a powerful tool for studying small silver clusters at very low temperatures.[12]

In the past few years, a great work has been done to unravel the mysteries trapped behind the silver clusters both by the experimental and theoretical point of view. Most of the efforts have been dedicated to the study of the structural, electronic, magnetic, and also optical properties. Considering the optical properties, the theoreticians performing electronic structure calculations have mostly restricted their investigations to the bare silver clusters[13–17] while in most practical cases, the clusters interact with their environment. This interaction has been poorly described and understood but however, it has got striking consequences on the physical properties of these clusters even though the matrix surrounding the cluster can be considered relatively "inert." This problem has been addressed mainly from the experimental side comparing the optical spectra produced by silver clusters in different rare gas matrices; however, it still remains an open question.[18] What is known until now in clusters embedded in Ar matrices is

a)Author to whom correspondence should be addressed. Electronic mail: manuel.pereiro.lopez@usc.es.

that the matrix effects produce two competing consequences. First, the matrix polarization forces the valence electrons of the cluster to be more confined than the valence electrons in the bare cluster.[19] This electron confinement produces a blueshift of the optical spectra. On the contrary, in Ref. 20 the influence of various rare gases on the optical spectra of the same selected small silver clusters was discussed. They showed that a variation of the gas matrices in the sequence $\mathrm{Ar} \mapsto \mathrm{Kr} \mapsto \mathrm{Xe}$ induces a redshift in the optical spectra as a consequence of the different values of their dielectric functions.

In this article, we have addressed this problem performing TDDFT calculations with the intention to obtain the optical spectra of the silver clusters embedded in a helium droplet. Moreover, we have compared them with the spectra of bare silver clusters and also with the reported experimental data in helium environment. We have studied only Ag_2 and Ag_8 clusters because of the reduced available experimental works in He droplets to compare with. Although the He environment is usually considered as an "inert" environment, we have found that it affects the interaction between silver cluster and helium producing a contraction of the Ag–He bonding length and also a confinement of the valence *s* electrons. The rest of the paper is organized as follows. In Sec. II, we present the structural details and the method employed to reach reliable structures. The theoretical background and the computational parameters used to obtain the optical spectra are also given in Sec. II. The results and discussion about the influence of the He nanodroplet in the optical properties of silver clusters is showed in Sec. III. We conclude with a brief summary of the main results obtained in this article in Sec. IV.

II. METHOD, STRUCTURAL, AND COMPUTATIONAL DETAILS

The ground-state structures of the bare silver clusters have been taken from our previous work on the static response of these clusters to an external electric field[21] and reoptimized with DEMON2K code[22] within the framework of an unrestricted Kohn–Sham quantum mechanics calculation. These structures are plotted in Fig. 1. In the case of Ag_2 molecule, our reported results for the binding energy and the bonding length are 1.56 eV and 2.66 Å, respectively. These data are in a very good agreement with the experimental results, which are 1.6 eV for the binding energy[23] and 2.53350 Å for the bonding length.[24]

For simulating the He environment, we first started performing a quantum mechanics geometry optimization of the Ag–He and He_2 clusters with DEMON2K code[22] and using the Broyden–Fletcher–Goldfarb–Shanno (BFGS) algorithm.[25] The bonding lengths provided by the optimization were d_{Ag-He}=4.14 Å and d_{He-He}=2.77 Å. It is also remarkable to note that the use of the generalized gradient approximation describes reasonably well the weak bonding interaction of He_2. Thus, both the bonding length (2.77 Å) and the binding energy (0.003 eV) are in a relatively good agreement with experiment[26] (2.98 Å and 0.001 eV, respectively). The bonding lengths calculated for He_2 and Ag–He

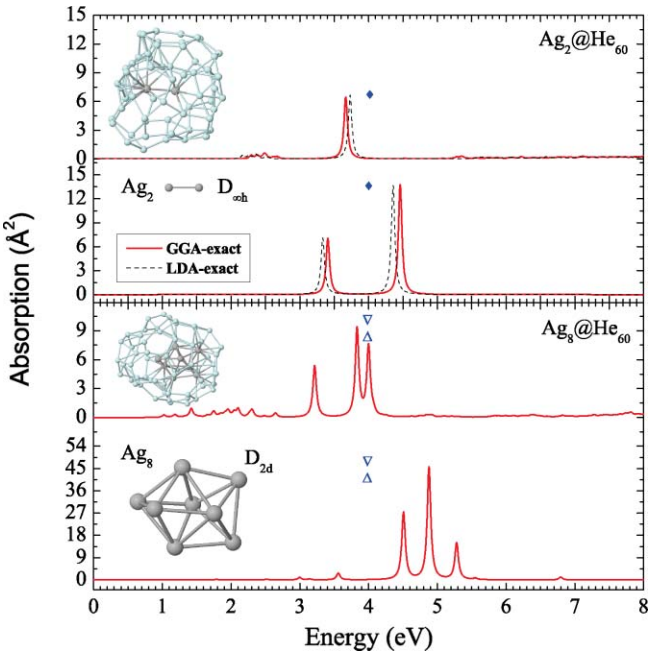

FIG. 1. Calculated excitation spectra of Ag_n and $Ag_n@He_{60}$ (n = 2, 8) clusters. The excitation spectra are given by the strength function defined in Eq. (2). We show the lowest-energy structures of the bare silver clusters and also the optimized structures of the silver clusters capped with He atoms. Position energies of the measured absorption peaks were taken from the available experiments of silver clusters embedded in nanoscopic helium droplets and they are represented by the symbols plotted in the figure. Thus, the unfilled triangle is for Ref. 42, the filled diamond symbol stands for data taken from Ref. 43 while unfilled inverted triangle corresponds to data reported in Ref. 44.

molecules gave us a slight indication at what distance the He atoms should be grouped around the silver clusters. With this in mind, in the initial process of the geometry optimization we have selected as guess geometry for the He matrix a buckyball structure composed of 60 He atoms and with the He–He and Ag–He bonding lengths given above. Note also that we have considered a He matrix composed of 42 He atoms but however for the reasons given in Sec. III and in Appendix B, we have decided to concentrate our efforts in the He matrix composed of 60 He atoms. The reason for using a buckyball structure is that at the experimental conditions, the helium gas condenses to superfluid helium nanodroplets and as far as we know, one of the best ways to simulate a droplet is with a buckyball structure. Thus, before the optimization process, the initial structures were constructed with the bare silver cluster in the center of the helium buckyball.

In this article, the silver clusters surrounded by He atoms have been relaxed with the BFGS algorithm as it is implemented in DEMON2K code. The whole cluster was treated using a quantum mechanics–molecular mechanics (QM/MM) scheme. The Hamiltonian describing the system is composed of the following terms:

$$H_{\mathrm{QM/MM}} = H_{\mathrm{MM}} + H_{\mathrm{QM}} + H_{\mathrm{QM-MM}}. \quad (1)$$

where H_{QM} is the *ab initio* quantum mechanics (QM) Hamiltonian for the quantum region, i.e., for the silver clusters enclosed into the He capsule. For this part of the

Hamiltonian, the orbital basis sets (ECP19lSD) (Ref. 27) were used in conjunction with the corresponding (A2-DZVP) (Ref. 27) auxiliary basis sets. In DEMON2K, the electron density is expanded in auxiliary basis functions which are introduced to avoid the calculation of the N^4 scaling Coulomb repulsion energy, where N is the number of the basis functions. Likewise, *ad hoc* relativistic effective-core potentials (ECP19lSD) have been used for describing the 28 inner electrons of each silver atom. The spin-unrestricted calculations were carried out at the generalized gradient approximation level to take the exchange-correlation effects into account.[28]

In Eq. (1), H_{MM} represents the molecular mechanics (MM) Hamiltonian for the rest of He atoms, i.e., the outer region used for the QM/MM approach. For this part of the Hamiltonian, the interaction between the He atoms was described by the universal force field.[29] Moreover, we used as a coupling Hamiltonian ($H_{\mathrm{QM-MM}}$) a simple mechanical embedding to describe interactions between the QM and MM parts. The MM subsystem does not directly influence the electronic structure of the QM part and the dynamical relationship between the QM and MM partitions was controlled with a synchronous method, i.e., the time steps are identical across the two partitions of the system.

During the optimization, the convergence criterion for the norm of the energy gradient was fixed to 3×10^{-4} a.u. while it was 10^{-7} a.u. for the energy and 10^{-5} a.u. for the charge density. The optimized structures surrounded by the helium atoms are plotted in Fig. 1. Some structural parameters are also reported in Table I. It is inferred from these data that the interaction of the He atoms with the silver clusters does barely alters the average first-neighbor distance between silver atoms with respect to the bare silver clusters.

In order to compute the electronic excitations induced by an external perturbation in the silver clusters, we have made use of a molecular implementation of the time-dependent density functional response theory restricted by the adiabatic approximation in the linear response regime.[30,31] So, hereafter the spectra showed in this article have been calculated with the OCTOPUS code.[30] The optical excitation spectra were given by the "strength function" as a function of the excitation energy ξ

$$S(\xi) = \sum_i f_i \delta(\xi - \xi_i), \tag{2}$$

where f_i is the oscillator strength expressed as

$$f_i = \frac{2}{3}(\xi_i - \xi_0) \sum_{n\in\{x,y,z\}} |\langle \Phi_0|\hat{n}|\Phi_i\rangle|^2. \tag{3}$$

The vertical excitation energy, $\xi_i - \xi_0$, is defined as the energy difference between the excited state, Φ_i, and the ground state, Φ_0. Generally speaking, the excitation spectra with nonzero oscillator strengths are usually called absorption spectra because the absorption cross section is proportional to the oscillator strengths.[32] To visualize the spectra presented below, the delta functions of Eq. (2) have been convolved with Lorentzian functions. The Lorentzian broadening has been set to 0.03.

The electron–ion interaction in Ag and He atoms was described through the Hartwigsen–Goedecker–Hutter (HGH) relativistic separable dual-space Gaussian pseudopotentials.[33] We restricted the calculations just to HGH pseudopotentials because the excitation spectra are usually quite insensitive to the changes in pseudopotentials.[34] Moreover, in the case of silver atoms, we have selected a pseudopotential which included 46 core electrons. The reason for making such a selection is twofold. First, the calculations take much less time than others with pseudopotentials considering less than 46 core electrons, and second, it has been reported in Refs. 35–37 that the transitions for silver clusters with a number of atoms less or equal to eight are mainly associated with *s* electrons, without any contributions from *d* electrons whatever the pseudopotential used. Thus, in Ref. 38 the large-core pseudopotential calculations are found to be in good agreement with the small-core pseudopotential calculations for the silver clusters with $n \leq 8$.

The exchange-correlation (XC) effects were treated at different levels of approximation. Thus, as shown in Fig. 1, we have also studied how the spectra is influenced by the XC functional. The different implementations for the XC effects of what we have made use are the exact exchange functionals handled by the optimized effective potential technique.[39] Thus, hereafter the LDA-exact and GGA-exact acronyms refer to the functionals with the correlation effects described by the local density approximation (LDA) or generalized gradient approximation (GGA), respectively, while the exchange is treated as exact.

The grid in real space to solve the Kohn–Sham equations consists in a sum of spheres around each atom of radius 5.5 Å and a mesh spacing of 0.23 Å. During the

TABLE I. Average first-neighbor distance of Ag bare clusters and their counterparts in helium environment. For the case of Ag@He clusters, we have also reported the average first-neighbor distance for Ag–He and He–He bondings. The symmetry of the point groups of Ag bare clusters was taken from Ref. 21 while for Ag@He clusters, the symmetries of the silver clusters and the He clusters surrounding them were determined from Ref. 51.

Ag			Ag@He					
				Point group	d (Å)			Point group
Cluster	Point group	d (Å)	Cluster	Ag cluster	Ag–Ag	Ag–He	He–He	He cluster
Ag_2	$D_{\infty h}$	2.66	$Ag_2@He_{60}$	$D_{\infty h}$	2.66	2.72	2.32	C_1
Ag_8	D_{2d}	2.88	$Ag_8@He_{60}$	D_{2d}	2.85	2.76	2.35	C_1
			$Ag_8@He_{42}$	D_{2d}	2.85	2.74	2.42	C_1

self-consistent field procedure, the convergence criterion for the absolute convergence of the electron density was fixed to 10^{-5}.

III. RESULTS AND DISCUSSION

The optical excitation spectra of Ag_n and $Ag_n@He_{60}$ ($n = 2, 8$) clusters are plotted in Fig. 1, where n represents the number of atoms belonging to the silver cluster. The optical spectra have been calculated with OCTOPUS code[30] for different XC functionals, namely, GGA-exact and LDA-exact as commented in Sec. II. There is no appreciable differences between both the GGA-exact and LDA-exact predicted spectra. The optical spectra for the LDA-exact functional have only been displayed for the Ag_2 and $Ag_2@He_{60}$ clusters to show the reader the small difference with GGA-exact spectra. In TM clusters, the exchange energy is usually one order of magnitude greater than the correlation energy. As a consequence, a good description of the electron–electron exchange effects is extremely important. The exact exchange functionals offer a great opportunity for retaining the electron–electron exchange effects at a level of high accuracy. For the above reasons, we have decided to concentrate our efforts in the calculated spectra provided by the GGA-exact functional, so hereafter the discussion only refers to the results obtained by this functional.

Although most of the experiments have been carried out in Ar matrices[6,37,40,41] for a large variety of silver clusters and just only a low percentage of them have been measured in He environment for a very reduced number of silver clusters,[42–44] however, we have observed in Fig. 1 that the calculated spectra in He environment fitted relatively good with the experimental data in comparison with the spectra produced by the bare silver clusters. Moreover, we also observe as a general trend a redshift of the $Ag_n@He_{60}$ spectra with respect to the corresponding Ag_n ones. The shifting of the spectra toward lower values in energy is purely a matrix effect. It was estimated for Ag_n clusters embedded in Ar matrices that the matrix causes a shifting of the absorption peaks from the bare cluster values of about 0.25 eV.[35] We have found that this value is generally greater (e.g., ∼0.79 eV for the silver dimer) in He environment than in Ar matrices. The redshifting has been attributed to the dielectric effect of the matrix.[20,45] Apart from this effect, our work indicates that there are other sources that contribute to the redshifting of the absorption peaks in the optical spectra of silver clusters embedded in He atoms and they are, namely, the contraction of the Ag–He bonding length and the confinement of the silver s electrons produced by the He atoms.

The dielectric effect produced by the helium environment in the optical spectra of silver clusters is rather inappreciable. The reason resides mainly in the small difference between the dielectric constant of helium and vacuum. To exemplify this point, we have plotted in Fig. 2 the absorption cross section predicted by the Mie–Gans (MG) theory[46,47] in the dipolar approximation for silver spheroids embedded in helium atoms and in vacuum.[48] The MG theory is a well-known classical theory describing the interaction between the electromagnetic waves and small ellipsoidal particles. More details about the MG theory and a derivation of the optical cross section for an ellipsoid embedded in a medium with dielectric function different from 1 is presented in Appendix A. We have taken the complex dielectric function of bulk silver from the experimental data.[49] Likewise, we have also selected from the experiment the dielectric constant of helium, $\epsilon_{He} = 1.02402$, at a temperature of 10 K and a pressure of 10 bar, because the spectra were measured close to these conditions. Structural details about these spheroids are reported in Table II.

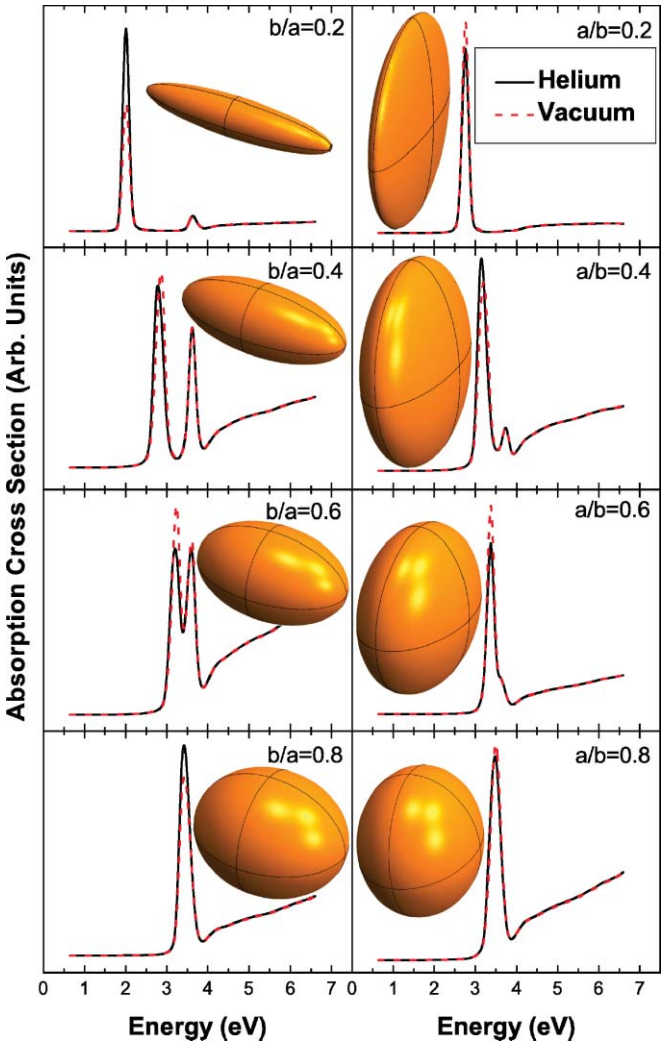

FIG. 2. Absorption cross section predicted by the Mie–Gans theory for silver spheroids of different shapes in helium environment and vacuum. The structural details of the spheroids are given in Table II. The volume of the spheroids is $V = \frac{4}{3}\pi abc = \frac{4}{3}\pi 10$ Å ^{3}.

TABLE II. Depolarization factors of an ideal spheroid ($a \neq b = c$) calculated for different b/a ratios. The b/a parameter determines the shape of the spheroid. For lower values of b/a, the spheroid adopt a prolate geometry while for higher values the spheroid becomes oblate.

b/a	L_1	$L_2 = L_3$	a/b	L_1	$L_2 = L_3$
0.2	0.056	0.472	0.2	0.750	0.125
0.4	0.134	0.433	0.4	0.588	0.206
0.6	0.210	0.395	0.6	0.478	0.261
0.8	0.276	0.362	0.8	0.396	0.302

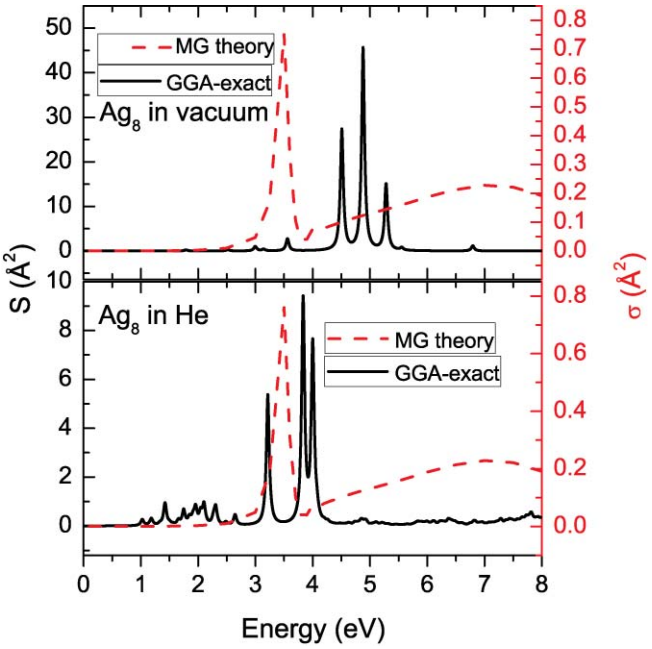

FIG. 3. Optical spectra predicted by both the Mie–Gans theory and TDDFT in the linear response approximation within the GGA-exact approximation. We compare both spectra in vacuum and in He environment for Ag_8 cluster. The structural details of the silver spheroids are given in Table III.

We observe in Fig. 2 that the difference of the optical cross section in helium and vacuum predicted by MG theory is rather small. We appreciate just only a small difference in the intensity of the main peaks but nothing else. It is also important to mention here that the two peaks appearing for the prolate and oblate spheroids are a consequence of sharing the same distance for two of the principal axes (see Appendix A for more details). In Fig. 3, we have also compared the optical spectra predicted by both the MG theory [see Eq. (A5)] and our TDDFT calculations. We have selected only the Ag_8 cluster because its shape is relatively well symbolized by an spheroidal particle, i.e., a prolate geometry. The structural details about the spheroids mimicking the Ag_8 clusters are collected in Table III. We first observe that the TDDFT spectra approaches to the MG prediction in He environment while for the vacuum the discrepancy is evident. Although the MG theory do not consider the quantum-mechanical nature of the nanoparticles, however; their predictions in He environment are quite realistic because they do not deviate too much from the TDDFT spectra. As a consequence, the dielectric effect which is produced by the substrate and which is also well-described by the MG theory cannot be the only source of the spectral shifting showed in Fig. 1 because its effect is relatively small.

TABLE III. Structural details of the Ag_8 and $Ag_8@He_{60}$ clusters studied in this work. The semiaxes of the clusters are represented by a, b, and c. The depolarization factors L_i ($i = 1$–3) were calculated according to Eq. (A2).

Cluster	a (Å)	b (Å)	c (Å)	L_1	L_2	L_3
Ag_8	2.175	1.890	1.890	0.297	0.352	0.352
$Ag_8@He_{60}$	2.174	1.890	1.890	0.297	0.352	0.352

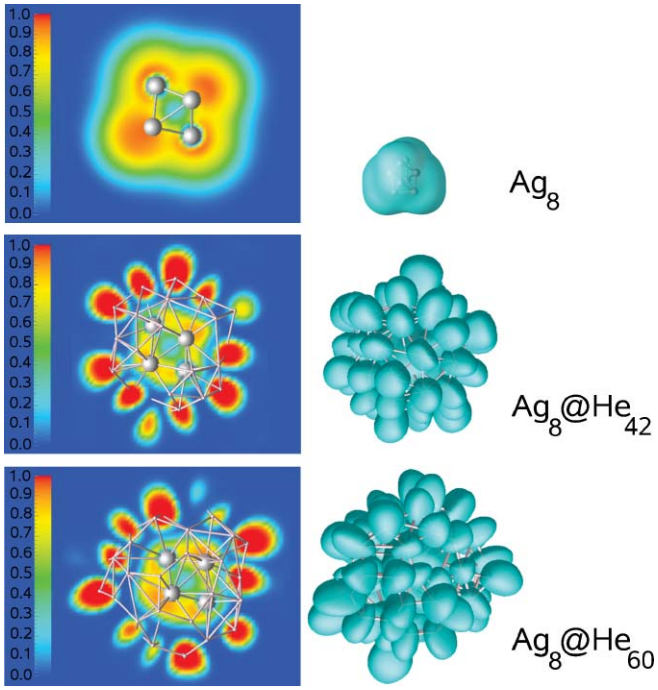

FIG. 4. Plot of the electron localization function for Ag_8, $Ag_8@He_{42}$, and $Ag_8@He_{60}$ clusters. On the left, we show the ELF projected in a plane passing through the center of the cluster. Moreover, we also show a three-dimensional plot of the ELF for an isosurface value of 0.29 on the right side of the figure.

According to our TDDFT calculations, the reason for the redshifted spectra resides in the decrease of the average Ag–He bonding length (see Table I) with respect to the distance of AgHe dimer (4.14 Å). In Fig. 4, we have plotted the electron localization function (ELF) calculated with the OCTOPUS code for Ag_8, $Ag_8@He_{42}$, and $Ag_8@He_{60}$ clusters. It can be seen how the ELF around the silver clusters evolves from a nonspherical form into a more spherical one. The spherical shape indicates the optimal conformation of the helium atoms around the silver cluster. That is the reason why we have selected the He_{60} matrix for simulating the He environment (see also Appendix B). Moreover, the diameter of the ELF around the Ag_8 silver cluster decreases with the enhancement of the helium atoms. Thus, the ELF diameter of the Ag_8 cluster in He_{60} environment is approximately 5.94 Å while for Ag_8 bare cluster, it is 9.90 Å. It is a consequence of the reduction in the average Ag–He bonding length (see Table I) which produces a relatively strong interaction between Ag and He atoms. Therefore, the helium atoms are producing a spatial confinement of the *s* electrons in silver clusters as shown in Fig. 4. It makes the energy of the higher occupied eigenvalues to be shifted to higher values in such a way that the energy difference involving the transitions to unoccupied levels is reduced.

IV. SUMMARY

In this work, we have studied from first-principles calculations the influence of He atoms in the optical spectra of small silver clusters. We have also investigated the influence of the XC effects in the optical spectra and we have found

that the LDA-exact and GGA-exact exchange functionals provide similar spectra. Overall, the optical spectra predicted by our TDDFT calculations within the GGA-exact approximation for $Ag_n@He_{60}$ clusters exhibit a relatively good agreement with the available experimental data in He nanodroplets. The He environment was simulated with a buckyball geometry and the bare silver clusters were implanted in the center of the buckyball. After that, a QM/MM simulation was used to optimize the structures. We have found that He environment affects the optical spectra shifting the peaks to lower values in energy. The redshift is attributed to the contraction of the Ag–He distance and consequently to a confinement of the *s* electrons in silver clusters. Moreover, the MG predictions combined with our TDDFT calculations also show that the dielectric effect produced by the He matrix is considerably less important in explaining the redshifting observed in the optical spectra of $Ag_n@He_{60}$ clusters with $n = 2$ and 8.

ACKNOWLEDGMENTS

The authors acknowledge the Centro de Supercomputación de Galicia for the computing facilities. M.P. acknowledges the Isabel Barreto program for financial support and the Department of Solid State Physics at the University of Łódź for its hospitality while this work was fulfilled. The work also was supported by both the Ministerio de Educación y Ciencia and Xunta de Galicia under projects No. MAT2009-08165 and No. INCITE08PXIB236052PR, respectively.

APPENDIX A: ABSORPTION CROSS SECTION IN THE MIE–GANS THEORY

The purpose of this appendix is to derive the absorption cross section predicted by the Mie-Gans theory[46,47] in the dipolar approximation for an ellipsoid embedded in a medium with dielectric function different from 1. Specially, in our case, the embedding medium is composed of helium atoms. The interaction of the electromagnetic waves with an ellipsoidal particle embedded in a medium is studied in the framework of the classical electrodynamics, assuming that the particle and the medium are continuous, homogeneous, and both are characterized by their dielectric function. We assume that the wavelength of the incident electromagnetic radiation is much greater than the principal axes of the ellipsoid. Hereafter, the equations are given in Gaussian units.

Let us consider an ellipsoid with the reference frame positioned in its center and where the semiaxes are of lengths a, b, and c. They are pictured in Fig. 2 for a volume $V = \frac{4}{3}\pi abc = \frac{4}{3}\pi 10\ \text{Å}^3$. If we applied an external electric field $\mathbf{E}^{\text{ext}}$ along one of the main axes ($i = 1, 2, 3$) of the ellipsoid, the total electric field $\mathbf{E}$ at any point inside the ellipsoid is given by

$$\mathbf{E}_i = \mathbf{E}_i^{\text{ext}} - 4\pi L_i \mathbf{P}_i, \tag{A1}$$

where $\mathbf{P}$ is the polarization vector per unit volume and L_i are geometric factors related to the depolarization effect. They are defined as

$$L_i = \int_0^\infty \frac{abc}{2(s+a^2)^{\alpha_i/2}(s+b^2)^{\beta_i/2}(s+c^2)^{\gamma_i/2}} ds, \tag{A2}$$

with $\alpha_i = (3, 1, 1)$, $\beta_i = (1, 3, 1)$, and $\gamma_i = (1, 1, 3)$. From the Maxwell's equations in the conditions commented above, it is easy to obtain that

$$\mathbf{P} = \frac{\tilde{\epsilon}_p - \epsilon_m}{4\pi\epsilon_m}\mathbf{E}, \tag{A3}$$

where ϵ_m is the dielectric function of the embedding medium which is supposed to be real (it represents the He environment in the main text), while the cluster material is characterized by a complex dielectric function $\tilde{\epsilon}_p = \epsilon_1 - i\epsilon_2$. Combining Eqs. (A1) and (A3), we can eliminate $\mathbf{E}$ and taking into account that $P_i V = \alpha_i \mathrm{E}_i^{\text{ext}}$, the resulting equation for the polarizability tensor is

$$\alpha_i = \frac{V}{4\pi} \frac{\tilde{\epsilon}_p - \epsilon_m}{L_i(\tilde{\epsilon}_p - \epsilon_m) + \epsilon_m}. \tag{A4}$$

For randomly oriented ellipsoids, we can average over the three spatial directions, so that the total polarizability is $\alpha = \frac{1}{3}\sum_{i=1}^{3}\alpha_i$. The absorption cross section described in the framework of classical optics is related to the polarizability by means of the formula $\sigma_{abs} = \frac{4\pi\xi}{\hbar c}\Re(i\alpha)$ in terms of the energy ξ. As a result of this derivation, the absorption cross section can be written as

$$\sigma_{abs}(\xi) = \frac{4\pi\xi abc}{9\hbar c}\sum_{i=1}^{3}\frac{\epsilon_2(\xi)\epsilon_m}{\{\epsilon_m + (\epsilon_1(\xi) - \epsilon_m)L_i\}^2 + (\epsilon_2(\xi)L_i)^2}. \tag{A5}$$

In the special case in which we can consider $\epsilon_2(\xi)$ nearly constant, the Mie–Gans resonance is satisfied under the condition $\epsilon_m + (\epsilon_1(\xi) - \epsilon_m)L_i = 0$. Consequently, the model predicts three resonance frequencies which can also be degenerated or not depending whether the lengths of the principal axes are either equal or not.

APPENDIX B: COMPARISON BETWEEN $Ag_8@He_{42}$ AND $Ag_8@He_{60}$ SPECTRA

Monte Carlo simulations have shown that for $Ag@He_n$ clusters, with $n \leq 100$, the number of He atoms which form the first coordination shell should be greater than 25.[50] Consequently, we have tested the Ag_8 cluster capped with 42 and 60 He atoms and we have found that the excitation spectrum of the cluster with 60 He atoms is the one which best fits to the experimental spectra as shown in Fig. 5. The main peak position calculated for $Ag_8@He_{60}$ cluster is in a very good agreement with the experimental result (3.97–3.99 eV) while in the case of $Ag_8@He_{42}$ the main excitations are shifted to lower values in energy. The reason, as commented in the main text, is a consequence of the more electron confinement in $Ag_8@He_{42}$ than in $Ag_8@He_{60}$ cluster. Thus, the average bonding length of Ag–He for $Ag_8@He_{42}$ cluster (2.74 Å) is lesser than the Ag–He distance for $Ag_8@He_{60}$ (2.76 Å). It is also reflected in the ELF plotted in Fig. 4. As shown, the ELF's diameter of the Ag_8 cluster in He_{42} environment is approximately 5.73 Å while for $Ag_8@He_{60}$ cluster the ELF's diameter of Ag_8 is close to 5.94 Å. Therefore, the shortening of the Ag–He distance produces an electron confinement in

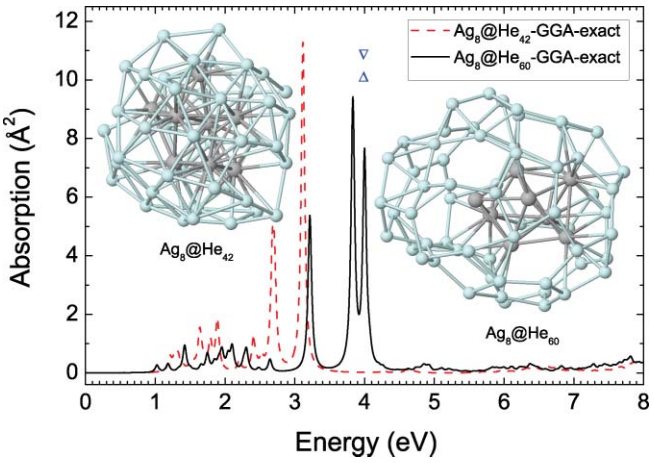

FIG. 5. Calculated excited spectra for $Ag_8@He_{42}$ and $Ag_8@He_{60}$ clusters. The symbols represent the measured peak positions and are the same as in Fig. 1. The geometries have been fitted to the size available in the figures and consequently they are not at the same scale. A quantitative detail about the structures is given in Table I.

$Ag_8@He_{42}$ greater than the $Ag_8@He_{60}$ case which induces a shifting to lower values in energy of the $Ag_8@He_{42}$ spectrum. In conclusion, a simulation considering an environment with 60 He atoms is more appropriate than others considering less than 60 He atoms.

[1] W. A. de Heer, Rev. Mod. Phys. **65**, 611 (1993).
[2] M. Brack, Rev. Mod. Phys. **65**, 677 (1993).
[3] F. Baletto and R. Ferrando, Rev. Mod. Phys. **77**, 371 (2005).
[4] C. C. Berry and A. S. G. Curtis, J. Phys. D: Appl. Phys. **36**, R198 (2003); Q. A. Pankhurst, J. Connolly, S. K. Jones, and J. Dobson, J. Phys. D: Appl. Phys. **36**, R167 (2003); P. Tartaj, M. del Puerto Morales, S. Veintemillas-Verdager, T. González-Carreño, and C. J. Serna, J. Phys. D: Appl. Phys. **36**, R182 (2003).
[5] M. Pereiro, D. Baldomir, J. Botana, J. E. Arias, K. Warda, and L. Wojtczak, J. Appl. Phys. **103**, 07A315 (2008).
[6] S. Fedrigo, W. Harbich, and J. Buttet, Phys. Rev. B **47**, 10706 (1993).
[7] M. Casida, *Recent Advances in Density-Functional Methods*, edited by D. P. Chong (World Scientific, Singapore, 1995), Part I, p. 459.
[8] W. M. C. Foulkes, L. Mitas, R. J. Needs, and G. Rajagopal, Rev. Mod. Phys. **73**, 33 (2001).
[9] J. Frank, *Introduction to Computational Chemistry* (Wiley, Chichester, 1999), Chap. IV.
[10] G. Onida, L. Reining, and A. Rubio, Rev. Mod. Phys. **74**, 601 (2002).
[11] D. Rayner, K. Athanassenas, B. Collings, S. Mitchell, and P. Hackett, *Theory of Atomic and Molecular Clusters: With a Glimpse at Experiments*, edited by J. Jellinek (Springer, Berlin, 1999), p. 371.
[12] J. A. Northby, Special issue on He-droplets [J. Chem. Phys. **115**, 10065 (2001)].
[13] M. L. Tiago, J. C. Idrobo, S. Ogut, J. Jellinek, and J. R. Chelikowsky, Phys. Rev. B **79**, 155419 (2009).
[14] G. F. Zhao, Y. Lei, and Z. Zeng, Chem. Phys. **327**, 261 (2006).
[15] V. Bonacic-Koutecky, V. Veyret, and R. Mitric, J. Chem. Phys. **115**, 10450 (2001).
[16] V. Bonacic-Koutecky, L. Cespiva, P. Fantucci, and J. Koutecky, J. Chem. Phys. **98**, 7981 (1993).
[17] K. Yabana and G. F. Bertsch, Phys. Rev. A **60**, 3809 (1999).
[18] F. Conus, V. Rodrigues, S. Lecoultre, A. Rydlo, and C. Félix, J. Chem. Phys. **125**, 024511 (2006).
[19] B. Gervais, E. Giglio, E. Jacquet, A. Ipatov, P.-G. Reinhard, and E. Suraud, J. Chem. Phys. **121**, 8466 (2004).
[20] S. Fedrigo, W. Harbich, and J. Buttet, Int. J. Mod. Phys. **6**, 3767 (1992).
[21] M. Pereiro, and D. Baldomir, Phys. Rev. A **75**, 033202 (2007).
[22] DEMON2K, A. M. Köster, P. Calaminici, M. E. Casida, R. Flores-Moreno, G. Geudtner, A. Goursot, T. Heine, A. Ipatov, F. Janetzko, J. M. del Campo, S. Patchkovskii, J. U. Reveles, D. R. Salahub, A. Vela (deMon developers, Montreal, 2006).
[23] V. Bonacic-Koutecky, L. Cespiva, P. Fantucci, and J. Koutecky, Z. Phys. D: At., Mol. Clusters **26**, 287 (1993).
[24] B. Simard, P. A. Hackett, A. M. James, and P. R.R. Langridge-Smith, Chem. Phys. Lett. **186**, 415 (1991).
[25] H. B. Schlegel, *Modern Electronic Structure Theory* (World Scientific, Singapore, 1995), Chap. VIII, pp. 459.
[26] J. O. Hirschfelder, *Intermolecular Forces* (Wiley, New York, 1967), Chap. VIII, pp. 466–467.
[27] See http://www.theochem.uni-stuttgart.de/pseudopotentials/index.en.html.
[28] J. P. Perdew, K. Burke, and M. Ernzerhof, Phys. Rev. Lett. **77**, 3865 (1996).
[29] A. K. Rappe, C. J. Casewit, K. S. Colwell, W. A. Goddard III, and W. M. Skiff, J. Am. Chem. Soc. **114**, 10024 (1992).
[30] M. A.L. Marques, A. Castro, G. F. Bertsh, and A. Rubio, Comput. Phys. Commun. **151**, 60 (2003).
[31] C. Jamorski, M. E. Casida, and D. R. Salahub, J. Chem. Phys. **104**, 5134 (1996).
[32] *Phosphor Handbook*, edited by W. M. Yen, S. Shionoya, and H. Yamamoto, (Taylor & Francis Group, New York, 2006), Chap. II.
[33] C. Hartwigsen, S. Goedecker, and J. Hutter, Phys. Rev. B **58**, 3641 (1998).
[34] M. A.L. Marques and S. Botti, J. Chem. Phys. **123**, 014310 (2005).
[35] J. C. Idrobo, S. Ogut, and J. Jellinek, Phys. Rev. B **72**, 085445 (2005).
[36] J. C. Idrobo, S. Ogut, K. Nemeth, J. Jellinek, and R. Ferrando, Phys. Rev. B **75**, 233411 (2007).
[37] M. Harb, F. Rabilloud, D. Simon, A. Rydlo, S. Lecoultre, F. Conus, V. Rodrigues, and C. Félix, J. Chem. Phys. **129**, 194108 (2008).
[38] M. Harb, F. Rabilloud, and D. Simon, Chem. Phys. Lett. **476**, 186 (2009).
[39] J. B. Krieger, Y. Li, and G. J. lafrate, Phys. Lett. A **146**, 256 (1990); Int. J. Quantum Chem. **41**, 489 (1992).
[40] C. Félix, C. Sieber, W. Harbich, J. Buttet, I. Rabin, W. Schulze, and G. Ertl, Chem. Phys. Lett. **313**, 105 (1999).
[41] C. Félix, C. Sieber, W. Harbich, J. Buttet, I. Rabin, W. Schulze, and G. Ertl, Phys. Rev. Lett. **86**, 2992 (2001).
[42] P. Radcliffe, A. Przystawik, T. Diederich, T. Döppner, J. Tiggesbäumker, and K.-H. Meiwes-Broer, Phys. Rev. Lett. **92**, 173403 (2004).
[43] A. Przystawik, P. Radcliffe, S. Göde, K. H. Meiwes-Broer, and J. Tiggesbäumker, J. Phys. B: At., Mol. Opt. Phys. **39**, S1183 (2006).
[44] T. Diederich, J. Tiggesbäumker, and K.-H. Meiwes-Broer, J. Chem. Phys. **116**, 3263 (2002).
[45] J. Andersen and E. Bonderup, Eur. Phys. J. D **11**, 435 (2000).
[46] G. Mie, Ann. Phys. **25**, 377 (1908).
[47] R. Gans, Ann. Phys. **37**, 881 (1912).
[48] J. C. Idrobo and S. T. Pantelides Phys. Rev. B **82**, 085420 (2010).
[49] *CRC Handbook of Chemistry and Physics*, edited by D. R. Lide, (CRC Press, New York, 2004), pp. 12–150.
[50] M. Mella, M. C. Colombo, and G. Morosi, J. Chem. Phys. **117**, 9695 (2002).
[51] See http://www.colby.edu/chemistry/PChem/scripts/ABC.html.